Environmental Science and Pollution Research (2022) 29:44732–44745
https://doi.org/10.1007/s11356-022-18901-z

RESEARCH ARTICLE

Sulfamethoxazole degradation by alpha-MnO_2/periodate oxidative system: Role of MnO_2 crystalline and reactive oxygen species

Zhijie Wang[1] · Jianguo Bao[1] · Jiangkun Du[1] · Liting Luo[2] · Guangfeng Xiao[1] · Ting Zhou[1]

Received: 22 July 2021 / Accepted: 23 January 2022 / Published online: 9 February 2022

Abstract

Pollutant degradation via periodate (IO_4^-) and transitional metal oxides provides an economical, energy-efficient way for chemical oxidation process in environmental remediation. However, catalytic activation of periodate by manganese dioxide and the associated mechanism were barely investigated. In this study, four MnO_2 polymorphs (α-, β-, γ- and δ-MnO_2) were synthesized and tested to activate IO_4^- for the degradation of sulfamethoxazole (SMX). The reactivity of different MnO_2 structures followed the order of α-MnO_2 > β-MnO_2 > γ-MnO_2 > δ-MnO_2, suggesting that the particular crystalline structure in α-MnO_2 would exhibit higher activities via IO_4^- activation. Herein, in α-MnO_2/IO_4^- system, 91.1% of SMX was eliminated within 30 min with degradation rate constant of 0.0649 min^{-1}, and the neutral pH exhibited higher efficiency in SMX degradation compared with acidic and alkaline conditions. Singlet oxygen ($^1O_2$) was unveiled to be the dominant ROS according to the results of electron paramagnetic resonance, chemical probes and radical quenching experiments, whereas $O_2^{\bullet-}$ and $^{\bullet}OH$ were mainly acted as a free-radical precursor. Six oxidation products were identified by LC–MS, and the elimination of sulfonamide bond, hydroxylation and direct oxidation were found to be the important oxidation pathways. The study dedicates to the mechanistic study into periodate activation over alpha-MnO_2 and provides a novel catalytic activation for selective removal in aqueous contaminants.

Keywords Manganese dioxides · Periodate · Superoxide radical · Singlet oxygen · Sulfamethoxazole

Introduction

Over the last few decades, antibiotic environmental residues have accelerated the development and spread of bacterial resistance in the aquatic environment, and the antibiotics are believed to pose potential risks to ecosystems and human even at a trace levels (Huang et al. 2020; Li et al. 2020a, b). Sulfamethoxazole (SMX) has been frequently used to prevent infections as a sulfonamide antibiotic. During the conventional wastewater treatment methods, the removal efficiency of SMX cannot achieve the desired effect due to its low biodegradability and long-term resistance in the environment (Chen and Wang 2021; Guo et al. 2020). Therefore, it is urgent to exploit effective methods and high-performance materials to deal with SMX from the aquatic environments (Li et al. 2020a, b; Yazdanbakhsh et al. 2020).

Among the various wastewater treatment technologies, the chemical oxidation process has built its position by achieving the complete degradation of toxic, recalcitrant compounds and microorganisms (Seid-Mohammadi et al. 2019). Commonly, the performance of chemical oxidation process is depended on the production of strong reactive intermediates, e.g., sulfate $\left(SO_4^{\bullet-}\right)$, hydroxyl ($^{\bullet}OH$) and iodate $\left(IO_3^{\bullet-}\right)$ via proper activation methods. Because oxidants themselves cannot directly destruct organic compounds, reactive radicals with much stronger oxidizing capacity should be generated by effective activation (Du et al. 2019a, b; Oh et al. 2016). For instance, H_2O_2 and persulfate activated by transition metal catalysts to produce highly reactive radicals have been shown to entirely

Responsible Editor: Ricardo A. Torres-Palma.

✉ Jiangkun Du
dujk@cug.edu.cn

[1] School of Environmental Studies, China University of Geosciences, Wuhan 430074, People's Republic of China

[2] State Key Laboratory of Magnetic Resonance and Atomic and Molecular Physics, National Center for Magnetic Resonance in Wuhan, Wuhan Institute of Physics and Mathematics, Innovation Academy for Precision Measurement Science and Technology, Chinese Academy of Sciences, Wuhan 430071, People's Republic of China

degrade the persistent organic pollutants to CO_2 and H_2O or convert them to a less toxic product (Antony et al. 2020; Du et al. 2019a, b). Therefore, more efforts should be taken to develop alternative oxidants with advanced activation technology and promote the otherwise sluggish degradation reactions.

Over the past decades, researchers have developed the application of periodate $\left(IO_4^-\right)$ -based chemical oxidation processes capable of removing recalcitrant organic contaminants from aquatic environment (Long et al. 2021). Although periodate is a strong oxidant (+ 1.60 V) thermodynamically, it requires efficient activation to produce highly reactive intermediates because periodate itself cannot achieve the oxidative decomposition of organic pollutants without activation process (e.g., UV irradiation, ultrasound, alkaline, freezing and reactive catalysts) (Bokare and Choi 2015; Choi et al. 2018; Gozmen et al. 2009; Lee et al. 2016; Wang et al. 2021a, b; Zong et al. 2021). Bendjama found that the degradation rate of the dye by UV/IO_4^- oxidation process was drastically advanced compared to direct UV alone because of the involvement of reactive iodine radicals in the degradation pathway (Bendjama et al. 2018). Lee et al. observed that the IO_4^-/US system provided effective and rapid remediation of the wastewater containing PFOA (Lee et al. 2016). In their study, $IO_2^{\bullet-}$ was likely to react with IO_4^- to form less effective radicals $IO_4^{\bullet}$, which can result in a decrease in PFOA degradation. Furthermore, Bokare and Choi used the KIO_4/KOH system to generate $^1O_2$ under neutral and near-alkaline conditions (Bokare and Choi 2015). For many approaches that have been studied, specific equipment and external energy consumption are needful for its activation. Therefore, transition metals might be one of the most promising options due to the high efficiency and easy management. Nevertheless, few relevant studies have been investigated, and the related mechanism deserves further exploration. For instance, Lee et al. employed bimetallic nanoparticles (nFe^0-Ni and nFe^0-Cu) to activate periodate, and $IO_3^{\bullet}$ was generated as dominant reactive radicals for contaminants degradation (Lee et al. 2014). Specially, manganese oxides activate periodate to generate singlet oxygen ($^1O_2$) and iodate radicals $\left(IO_3^{\bullet}\right)$. The oxidative reactivity of manganese oxidants followed the order of $MnO_2 > Mn_3O_4 > Mn_2O_3$ (Du et al. 2020).

Manganese dioxide (MnO_2), as the most strong nature oxidants and the most-attractive oxide materials, is environmental friendly, relatively inexpensive, and rich natural abundance (Huang et al. 2018; Taujale et al. 2016). In nature, MnO_2 can be found in many phase structures such as α-, β-, γ- and δ-MnO_2, and all these polymorphs are constituted of MnO_6 octahedral units (Huang et al. 2018). According to previous studies, it was evidenced that MnO_2 in various polymorphs showed the different catalytic and oxidative reactivity due to its physical and chemical properties (Li et al. 2018). Huang et al. discovered that the interfacial conductivity of the manganese dioxide could be important in the oxidative reaction because higher electrical conductivity will result in the faster electron transferability (Huang et al. 2018). Moreover, Saputra et al. found that the exposure of MnO_6 edges in two-tunnel structure will show higher activity than the single-tunnel structure by investigating the structure of α-, β- and γ-MnO_2 (Saputra et al. 2012). In previous studies, different MnO_2 polymorphs were commonly used to effectively activate oxone or persulfate to degrade contaminants in heterogeneous system. For instance, the oxidative reactivity of MnO_2 with different phase structures was tested in heterogeneous activation of PMS for phenol degradation and followed in the order of α-MnO_2 > γ-MnO_2 > β-MnO_2 (Saputra et al. 2013). In addition, one-dimensional MnO_2 with different crystallographic phases, α- and β-MnO_2 were investigated to activate PDS for selective degradation of organic pollutants, and singlet oxygen ($^1O_2$) was revealed to be the dominant ROS in this study (Zhu et al. 2019). Therefore, based on the previous research, we have found that MnO_2 was an efficient advanced oxidation system for degradation of sulfanilamide. However, the different crystallographic MnO_2 structures may show different activities in activation of periodate for organic pollutants degradation. Meantime, the relevant researches were rarely reported, and the underlining mechanism like electrochemical characterization and degradation product has not yet been elucidated.

Herein, in an effort to demonstrate the different MnO_2 polymorphs activating IO_4^-, we synthesized α-, β-, γ- and δ-MnO_2 by a hydrothermal method and evaluated their efficiency for IO_4^- activation. As one of the most frequently used sulfamethoxazole antibiotics, SMX was used as a chemical probe to quantify the oxidative reactivity of MnO_2. The objectives of this study are to discuss the several reaction factors and the catalyst reusability, identify and characterize major SMX transformation product(s), propose the catalytic degradation mechanism of the oxidation system via main reactive radicals. The exploration of MnO_2/IO_4^- system provides distinctive insight into the working mechanism of periodate-based chemical oxidation process and offers another prototype for the precise and rational design of more efficient activator for the degradation of aqueous antibiotic contaminants.

Experimental section

Chemicals

Sulfamethoxazole (SMX), ciprofloxacin (CIP), sulfamerazine (SMR), furfuryl alcohol (FFA), acetonitrile (ACN, 99.9%), rhodamine B (RhB), p-benzoquinone (BQ), methylene blue (MB) and phenol (C_6H_5OH) were purchased from Aladdin Industrial Corporation. Acid

Orange 7 (AO7), 5-methylisoxazole (C_4H_5NO, 95%), 2,2,6,6-tetramethylpiperidine (TEMP) and 5,5-dimethyl-1-pyrrolidine-N-oxide (DMPO) were supplied by Shanghai Macklin Biochemical Co., Ltd. Sodium periodate ($NaIO_4$), potassium permanganate ($KMnO_4$), ammonium persulfate ($(NH_4)_2S_2O_8$), manganese sulfate monohydrate ($MnSO_4 \cdot H_2O$), bisphenol S (BPS), sulfanilamide ($C_6H_8N_2O_2S$), sodium chloride (NaCl), sodium carbonate (Na_2CO_3), *tert*-butyl alcohol (TBA, 99.7%), phosphoric acid (H_3PO_4), sodium fluoride (NaF) were provided by Sinopharm Chemical Reagent Co,. Ltd. All the solutions prepared using deionized (DI) water (> 18.25 MΩ).

Activators preparation and characterization

α-, β-, γ- and δ- types of MnO_2 polymorphs were prepared by a hydrothermal method (Yang et al. 2020), and the reaction was based on the redox reactions of Mn^{2+} ions with oxidizing agent. Detailed procedures are presented in Supporting Information (Text S1). The prepared α-, β-, γ- and δ-MnO_2 samples were characterized by X-ray diffraction (XRD, Bruker D8 DISCOVER) and X-ray photoelectron spectroscopy (Thermo Scientific K-Alpha).

Experiment procedure and analytical methods

Experiments were conducted in 250-ml glass flask under magnetic stirring (rotary speed = 500 rpm) at an ambient temperature, and then, the pH of the solution was adjusted with 1 M H_2SO_4 or NaOH except for experiments investigating the pH effect. The reaction temperature was kept at 25℃ through a thermostat circulator. Typically, $NaIO_4$ (2 mM) was spiked into 100 ml solution containing SMX (10 mg/L) and 0.1 g/L of the respective activator to start the degradation reaction. Besides, the photocatalytic experiment has been performed using a source of visible light, which was placed at a height of 10 cm from the solution. As the oxidation reaction proceeded, aliquots of 1 ml were withdrawn at different intervals, immediately mixed with 1 ml sodium thiosulfate to terminate the reaction, and samples were filtered by a nylon membrane (0.22 μm) for HPLC analysis. For the recycle tests of the catalysts, after each run, the catalyst was obtained by filtration and washed with DI water and ethanol several times, and then dried at 60℃ for 8 h. All experiments were performed in at least duplicate.

To quantitatively examine the oxidative reactivity of different parameters in MnO_2/periodate system, rate constants for the oxidative reactivity (k) were calculated based on the pseudo-first-order kinetics (Eq. 1).

$$\ln\left(\frac{C_0}{C_t}\right) = K_{obs}t \quad (1)$$

where C_0 is the SMX concentration before the reaction, C_t is the concentration at time t min of SMX in the MnO_2/periodate system, and K_{obs} represents the pseudo-first-order rate constant (min^{-1}).

The concentration of sulfamethoxazole was analyzed using a RIGOL L-3000 HPLC with a UV detector set at λ = 278 nm. AC-18 column (5 μm, 4.6 × 250 mm) was used to separate the organics, while the mobile phase with a flow rate of 1 ml/min eluent, which consisted of a binary mixture of 45% acetonitrile and 55% water. The reactive radicals generated by periodate were observed on a JES-FA200 electron paramagnetic resonance spectrometer measurement using 5,5-dimethyl-1-pyrroline N-oxide (DMPO) or 2,2,6,6-tetramethyl-4-piperidinol (TEMP) as spin-trapping agent. UV–Vis absorption spectra were measured in a 1-cm quartz cuvette using a METASH UV-5500(PC) spectrophotometer. Electrochemical characterization was performed with an VMP-3 (Bio-Logic SAS, France). In addition, degradation products of SMX were determined using LC-Q-TOF–MS analysis (Text S2).

Results and discussion

Characterization of catalyst

The different structures of MnO_2 samples were confirmed by the XRD patterns, as shown in Fig. 1a and b, which corresponded well to α-MnO_2 (JCPDS 44–0141), β-MnO_2 (24–0735), γ- MnO_2 (14–0644) and δ-MnO_2 (80–1098), respectively, according to the previous researches (Deng et al. 2017; Jia et al. 2016; Li et al. 2018; Saputra et al. 2013; Wang et al. 2015; Yang et al. 2020). No miscellaneous peaks and noticeable deviation appear in the pattern, clearly suggesting the purity of the catalyst. Compared to α- and β-MnO_2, other crystal structure featured broader peaks and low intensity of diffraction peak, indicating the lower crystallinity and small grain sizes. As depicted in Fig. 1a, α-MnO_2 did not change significantly after the reaction, suggesting that the crystal form of α-MnO_2 is relatively stable in the whole reaction. In general, α-, β-, γ- and δ-MnO_2 structures are all formed by the chains of MnO_6 octahedra, which are interlinked in different ways and constructed tunnels or interlayers with the gaps of different dimensions (Li et al. 2018; Saputra et al. 2013). Thereinto, α-MnO_2 was composed of double chains of edge-sharing MnO_6 octahedra with (2 × 2) and (1 × 1) tunnels (Zhu et al. 2019). β-MnO_2 consists of single strands of edge-sharing MnO_6 octahedra with (1 × 1) tunnel, whereas γ- MnO_2 was provided with random intergrowth of (1 × 1) and (1 × 2) tunnel forms (Yang

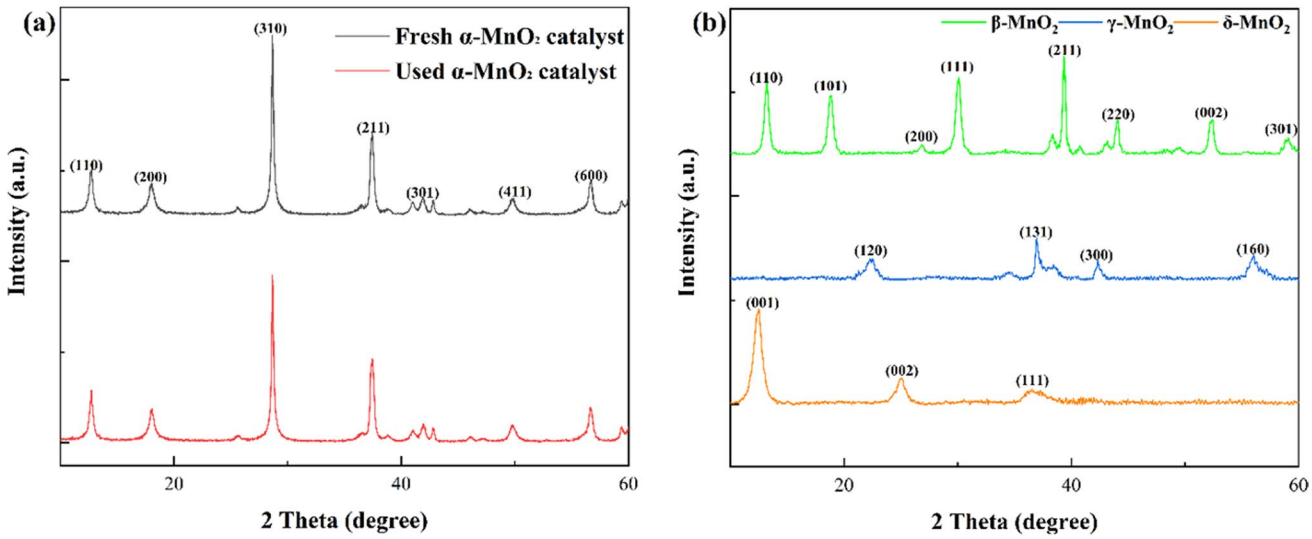

Fig. 1 (a) XRD pattern of α-MnO_2 in α-MnO_2/IO_4^- system before and after reaction, (b) XRD pattern of β-, γ- and δ-MnO_2 samples

et al. 2020). With the presence of K^+ and H_2O in the mezzanines, δ-MnO_2 was constructed with the 2D layer structure (Devaraj and Munichandraiah 2008). Therefore, periodate activated by different crystallographic MnO_2 may manifest different oxidation activities due to the difference among the structures of MnO_2.

Periodate activation on different crystalline MnO_2 for SMX degradation

Figure 2a shows the adsorption and degradation profiles of sulfamethoxazole against time on various MnO_2 materials. For different MnO_2 structures without the presence of periodate, control experiments showed negligible adsorption of SMX at less than 5% in 120 min, and IO_4^- alone cannot degrade SMX. With the combination of MnO_2 and periodate, the performance of MnO_2/IO_4^- system was obviously better than others, and the activities of four MnO_2 samples were significantly different. For the δ-MnO_2/IO_4^- process, it showed the minimum degradation rate of SMX, and less than 60% SMX removal was achieved after 120 min. However, SMX degradation could nearly reach 95% within 120 min in the α-MnO_2/IO_4^-, β-MnO_2/IO_4^- and γ-MnO_2/IO_4^- system. Figure 2b shows that the SMX degradation curves

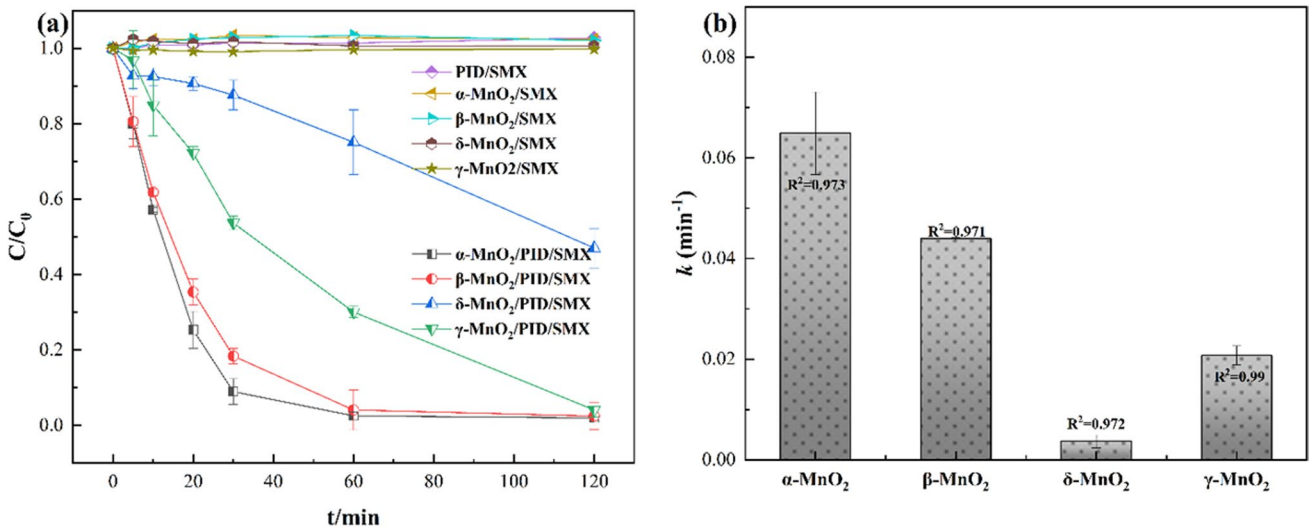

Fig. 2 (a) Sulfamethoxazole degradation on different MnO_2 samples, (b) pseudo-first-order oxidation rate constants (*k*) of SMX by different MnO_2 structures. Reaction conditions: $[\alpha\text{-}MnO_2]_0 = [\beta\text{-}MnO_2]_0 = [\gamma\text{-}MnO_2]_0 = [\delta\text{-}MnO_2]_0 = 0.2$ g/L, $[\text{Sulfamethoxazole}]_0 = 10$ mg/L, $[IO_4^-]_0 = 2.0$ mM, pH = 7

of different MnO_2 polymorphs can be fitted by the first-order kinetics. As shown in Fig. S1, α-MnO_2 presented high reactivity toward SMX in both dark and light conditions, with a similar *k* value of 0.0649 min^{-1} (without light) and 0.0698 min^{-1} (with light), respectively. Therefore, α-MnO_2 exhibited weak photocatalytic activity under solar light due to the slight enhancement of the *k* value upon light irradiation. As it can be seen, the catalytic activity of periodate activated by different crystallographic MnO_2 decreases in the order: α-MnO_2 > β-MnO_2 > γ-MnO_2 > δ-MnO_2. Compared to structure of α-MnO_2 and β-MnO_2, α-MnO_2 feature (2 × 2) tunnels will show higher catalytic activity than (1 × 1) channels structured β-MnO_2 due to the more exposure of MnO_6 edges (Saputra et al. 2013). In addition, the difference of various MnO_2 surface areas and active sites may also be result in the differences of catalytic activities according to the previous studies (Liu et al. 2009). Thus, under α-MnO_2/IO_4^- system, α-MnO_2 could possess higher surface area and more active sites than others, which could deduce that the related radical species may be bounded to the catalytic surface and SMX degradation may partly occur on the surface of catalyst (authenticated in Sect. 3.4).

Effect of Experimental conditions and Repetitive Use of α-MnO_2

To further understand the impacts of SMX removal by α-MnO_2/periodate process, several experimental factors on SMX degradation were investigated, including the pH, periodate concentration and α-MnO_2 dosage. Previous studies reported that the species of periodate and SMX could be strongly influenced by solution pH (Du et al. 2020; Lee et al. 2014; Sun et al. 2020). In Fig. 3a, the initial of solution pH, i.e., from pH 5 to 7, the SMX degradation slightly increased from 0.0605 to 0.0649 min^{-1}. The result in this phenomenon could be attributed to the predominant form of SMX in the acidic condition. Under different pH values, SMX exists in different forms, including protonate, non-protonated and deprotonated forms, and deprotonated form would result in the higher activation of periodate at pH = 7 (Qi et al. 2014). When the pH was further increased to 9, the SMX degradation significantly inhibited in the α-MnO_2/IO_4^- system, which could be due to the periodate speciation change depending on pH. Therefore, it was unfavorable for the activation of periodate species due to the transformation from IO_4^- ($E^0 = +1.6$ V) to $H_2I_2O_{10}^{4-}$ ($E^0 = +0.7$ V) as the solution pH shifted from the neutral to alkaline zone (Eqs. 2–3) (Li et al. 2017). Moreover, compare to the dimerized species ($H_2I_2O_{10}^{4-}$), IO_4^- species could be more efficient for $^1O_2$ generation (Bokare and Choi 2015). Although the SMX removal process was influenced at pH = 9, almost 95% of the contaminants was still eliminated after 120 min, suggesting that the α-MnO_2/IO_4^- system was suitable for a wide pH range.

$$2H_3IO_6^{2-} \leftrightarrow H_2I_2O_{10}^{4-} + 2H_2O \quad (2)$$

$$H_4IO_6^- \leftrightarrow IO_4^- + 2H_2O \quad (3)$$

As indicated in Fig. 3b, in order to obtain the optimum α-MnO_2 dosage, SMX degradation rate was investigated with different α-MnO_2 dosage from 0.1 g/L to 0.3 g/L, achieving 0.031 min^{-1}, 0.0649 min^{-1} and 0.1331 min^{-1}. An increase in catalyst dosage from 0.1 g/L to 0.2 g/L led to an increase in the degradation from 60% to 91.1% within 30 min, which suggests that more active sites on the surface of catalyst were accessible for periodate activation (Chadi et al. 2019). But SMX degradation did not show obviously increase when further increasing catalytic dose from 0.2 g/L to 0.3 g/L. Therefore, the reasonable dosage of α-MnO_2 was 0.2 g/L. To assess the effect of initial periodate concentration in SMX degradation, the degradation efficiency in α-MnO_2/IO_4^- system is detailed in Fig. 3c. When the IO_4^- concentration was set as 2 mM, the removal efficiency of SMX markedly increased from 48.2% with 0.5 mM of IO_4^- to 91.1% with 2 mM of IO_4^- in 30 min. The result suggests that the more extensive contact between IO_4^- and active sites was facilitated by the increased concentration of IO_4^-. Particularly, when the dose of IO_4^- reached to 3 mM, catalyst provides a limited number of active sites; thus, the increase of IO_4^- from 2 to 3 mM did not enhance the SMX degradation (Long et al. 2021). Hence, 2 mM IO_4^- was selected as the appropriate dose in the experiment.

As known, the stability and reusability of catalyst are an important factor for its potential applications. To evaluate the recycle utilization performance of as-obtained α-MnO_2, several cycling experiments were further conducted with simple process of filtration and drying. As displayed in Fig. 3d, α-MnO_2 could be repeatedly used to activate periodate in the second round, and the SMX removal efficiency remained approximately 97% within 60 min. Thereafter, the SMX removal efficiency gradually decreased to 86.1 and 78.4% in 60 min, respectively, for the third and fourth rounds. On the one hand, the decrease activity of the activator was possibly attributed to the oxidation product adsorption on the activator surface and the slight manganese leaching (Fig. S2) (Li et al. 2020a, b; Wang et al. 2015). On the other hand, based on the XPS of the fresh and used α-MnO_2, the oxidation–reduction of Mn species may also explain the inevitable decrease of catalytic activity in aqueous α-MnO_2/IO_4^- suspensions over four cycles. Nevertheless, the XRD image after the reaction can be seen that the crystalline phase of α-MnO_2 was still observed, indicating the good stability of α-MnO_2.

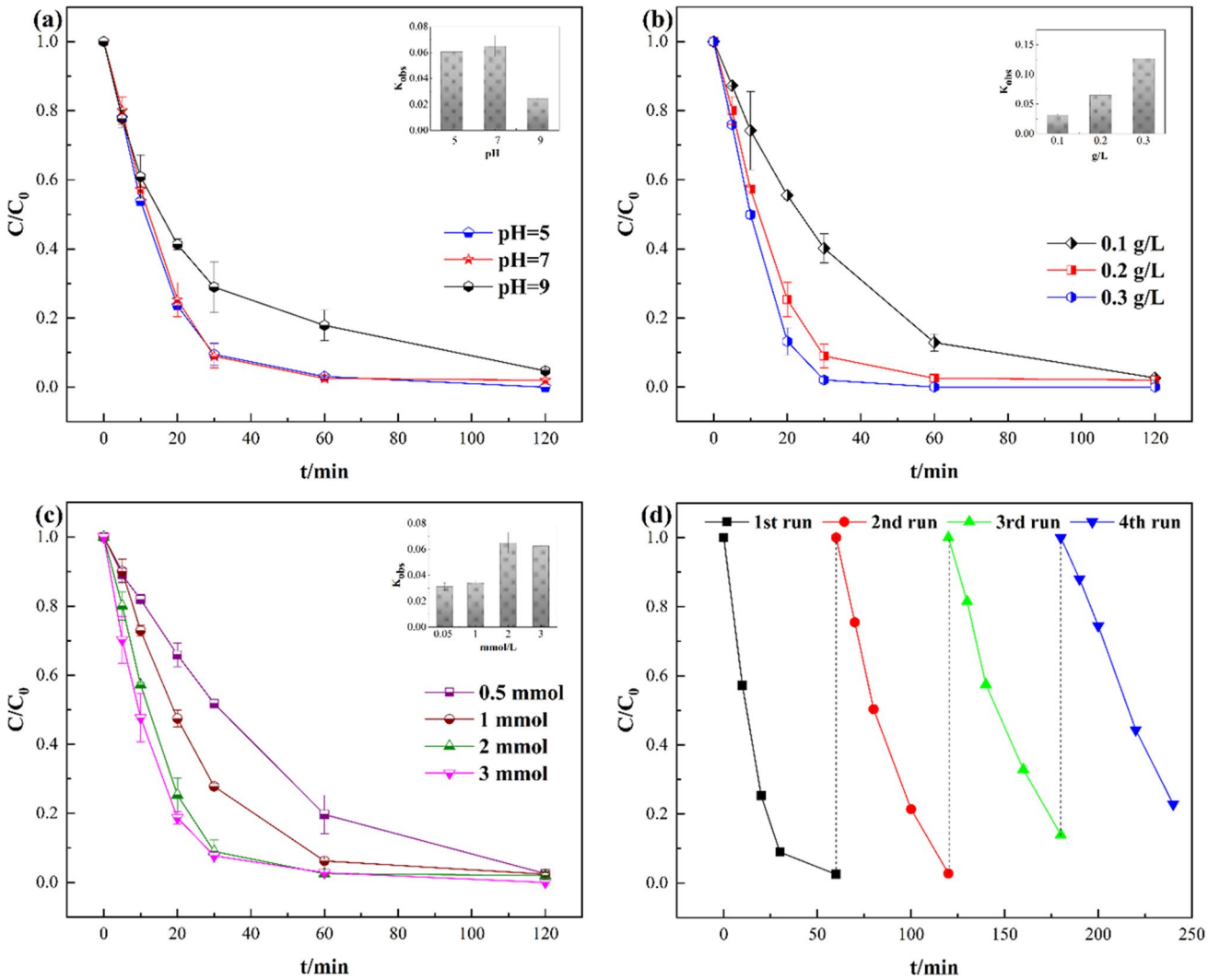

Fig. 3 Effect of (a) solution pH, (b) catalyst dosage, (c) IO_4^- concentration on SMX degradation by the α-MnO_2/IO_4^- system and (d) reusability of α-MnO_2. Reaction conditions: [Sulfamethoxazole]$_0$ = 10 mg/L, [IO_4^-]$_0$ = 2 mM (for a, b, and d), [α-MnO_2]$_0$ = 0.2 g/L (for a, c, and d), pH = 7 (for b-d)

Identification of the SMX Transformation Product

Transformation products of SMX in the α-MnO_2/IO_4^- system were analyzed using LC-Q-TOF–MS. Based on the analysis, six major degradation intermediates were identified, including 4-acetylbenzenesulfonamide (*m/z* 276), sulfanilic acid (*m/z* 158), malonic acid (*m/z* 105), 5-methylisoxazol-3-amine (*m/z* 99), oxalic acid (*m/z* 90), ammonium formate (*m/z* 64). The detailed information and MS^2 spectra of oxidation products are shown in Table 1 and Figs. S3–8. According to the integrated degradation and previous studies, the main degradation steps are proposed in Fig. 4, including the elimination of sulfonamide bond, hydroxylation and direct oxidation (Chen and Wang 2021; Li et al. 2020a, b; Wang et al. 2020; Zong et al. 2021). For the pathway I, the cleavage of S–N bond resulted in SMX molecule produced TP4 and TP6; the intermediate TP4 would further decompose to TP2. As depicted in Fig. S9, the time-dependent concentrations of 5-methylisoxazole gradually decreased during the degradation of SMX, while for sulfanilamide, its concentration slightly decreased. Therefore, the degradation of 5-methylisoxazole supported the proposed pathway I with the involvement of TP4. According to the previous CuO_x/persulfate system (Lalas et al. 2021), the pathway II could be identified by hydroxylation on the benzene ring, followed by cleavage of the isoxazole, resulting in the formation of TP7. In pathway III, two types of organic acid were generated during the degradation of SMX, including malonic acid and oxalic acid, which indicated the transformation of SMX. At last, the relevant transformation products were converted to carbon dioxide and

Table 1 Accurate mass and structures of SMX and its oxidation products

Product ID	Elemental formula	m/z	RT/min	Proposed structure
TP1	$C_{10}H_{11}N_3O_3S$	254	2.09	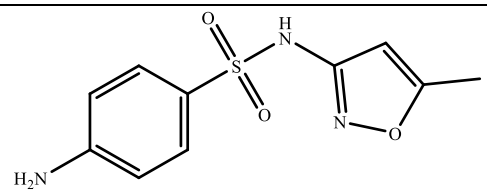
TP2	CH_5NO_2	64	1.32	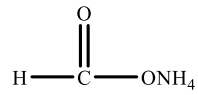
TP3	$C_2H_2O_4$	90	1.31	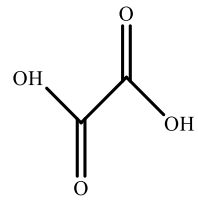
TP4	$C_4H_7ON_2$	99	1.69	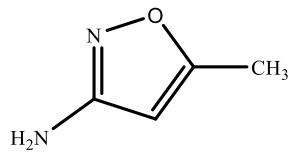
TP5	$C_2H_4N_2O_3$	105	1.32	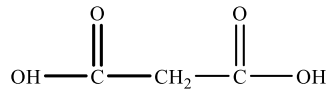
TP6	$C_6H_8O_2NS$	158	1.31	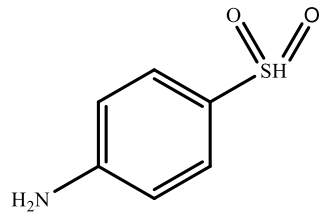
TP7	$C_{16}H_{22}N_2O_2$	276	5.11	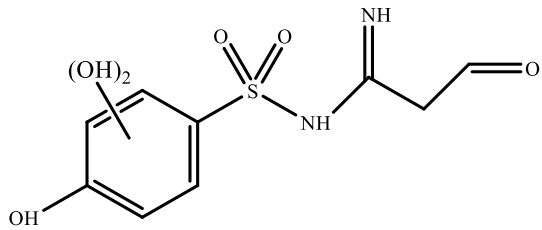

water through a serious of chemical reactions, which can be confirmed that the degradation and mineralization of SMX indeed occurred.

The Mechanism for Activating Periodate

Identification for the involved reactive species via chemical quenching experiments is of great significance to

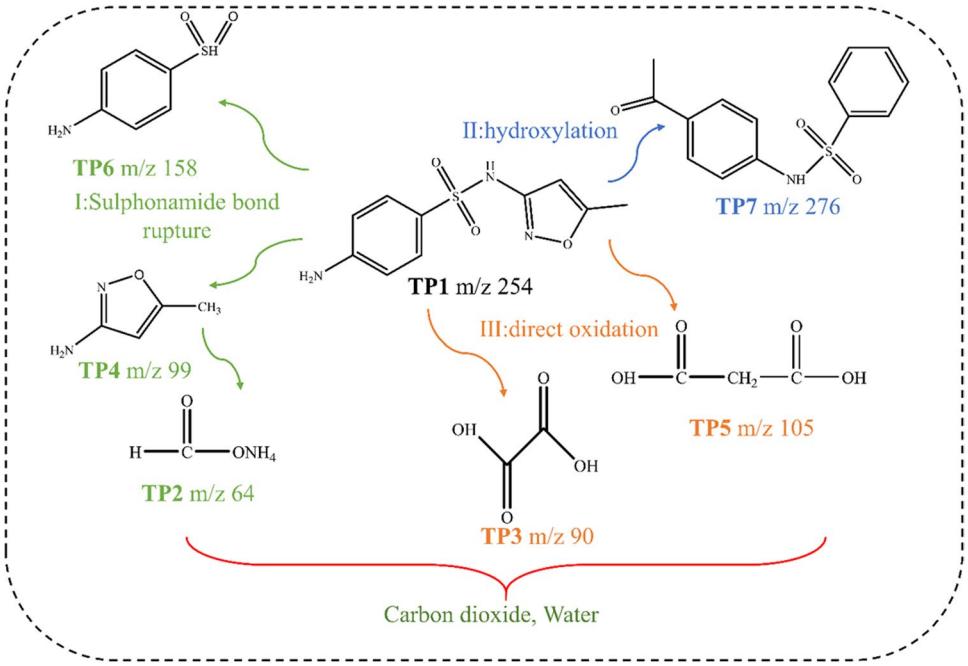

Fig. 4 Possible pathways of SMX oxidation by the α-MnO_2/IO_4^- system

understand the underlying mechanism in the α-MnO_2-activated IO_4^- oxidation process. As shown in Fig. 5a, the addition of 10 mM or 200 mM tert-butyl alcohol (k_2(TBA, $^{\bullet}$OH) = 3.8–7.6 × 10^8 M^{-1} s^{-1}) showed an adverse impact on SMX degradation, suggesting that $^{\bullet}$OH may exist in the process (Zong et al. 2021). On the contrary, the inhibition effect of TBA indicates that $IO_3^{\bullet}$ should not be the dominant ROS in SMX degradation because TBA cannot be reactive toward $IO_3^{\bullet}$ (Chadi et al. 2019). Additionally, when nitrobenzene (NB) was used as the chemical probe for $^{\bullet}$OH (k_2(NB, $^{\bullet}$OH) = 3.9 × 10^9 M^{-1} s^{-1}); accordingly, the removal efficiency of NB (42%) is observed in Fig. S10, which indicated that a small amount of $^{\bullet}$OH was produced (Zhu et al. 2019). Moreover, the α-MnO_2/IO_4^- reaction was carried out in the presence of chloride ion that was reported to be reactive with hydroxyl radicals to produce hypochlorous acid radicals (k_2(Cl^-, $^{\bullet}$OH) = 4.3 × 10^9 M^{-1} s^{-1}) (Buxton et al. 1988) (Eq. 4). As depicted in Fig. S11, the observation that degradation of SMX exhibited negligible change after the addition of Cl^- did not support the role of $^{\bullet}$OH as a dominant ROS in the α-MnO_2/IO_4^- system because $ClOH^{\bullet-}$ has lower activity than $^{\bullet}$OH (Wang and Wang 2020). Meanwhile, the presence of $^{\bullet}$OH in the aqueous phase can also be verified by using EPR experiment, whereas no certain signal in the reaction was observed by using DMPO as a spin trapping agent. In accordance with above results, the inhibition effect of TBA could be considered as a probability that TBA as a hydrophilic compound has a lower affinity to the surfaces of catalyst. Therefore, phenol (k_2(Phol, $^{\bullet}$OH) = 6.6 × 10^9 M^{-1} s^{-1}) was introduced to quench the radicals on the catalytic surface as a hydrophobic compound (Yang et al. 2015). The addition of phenol significantly quenched the SMX degradation, indicating that $^{\bullet}$OH may be formed on the surface of α-MnO_2 (Fig. 5a). Thus, fluoride was subsequently added to enhance the generation of free $^{\bullet}$OH radical in solution since the fluoride ions present in the Helmholtz layer are able to promote the desorption of surface-bound $^{\bullet}$OH radicals into solution from the surface of α-MnO_2, through a fluorine hydrogen bond (Xu et al. 2007). As fluoride concentration in the Helmholtz layer is increased, the rate of desorption of surface-bound $^{\bullet}$OH is promoted, thus accelerating the degradation of SMX in solution. In the presence of NaF, the reaction rate of SMX degradation was increased from 0.0857 min^{-1} to 0.101 min^{-1} in 30 min, which could further determine the existence of surface-bound $^{\bullet}$OH during the oxidative removal of SMX (Fig. 5a). All in all, the contribution of $^{\bullet}$OH and $IO_3^{\bullet}$ to contaminant removal is supposed to be insignificant in the $\alpha - MnO2/IO_4^-$ system, and the underlying mechanism of IO_4^- activation by α-MnO_2 could be dominated by a non-radical pathway.

$$Cl^- + OH \rightarrow ClOH^- \quad (4)$$

Considering the production of $^{\bullet}$OH on the catalyst surface, potassium dichromate ($K_2Cr_2O_7$) was subsequently employed to identify the possible electron transfer for the formation of ROS in aqueous phase (Huang and Zhang 2019). As shown in Fig. 5b, the removal efficiency of SMX was obviously inhibited with 2 mM $K_2Cr_2O_7$, suggesting that the oxidative system could generate ROS through solution-phase electrons transfer. As known, the dominant ROS of some periodate-based processes on contaminant degradation was frequently implicated to the role of singlet oxygen ($^1O_2$)

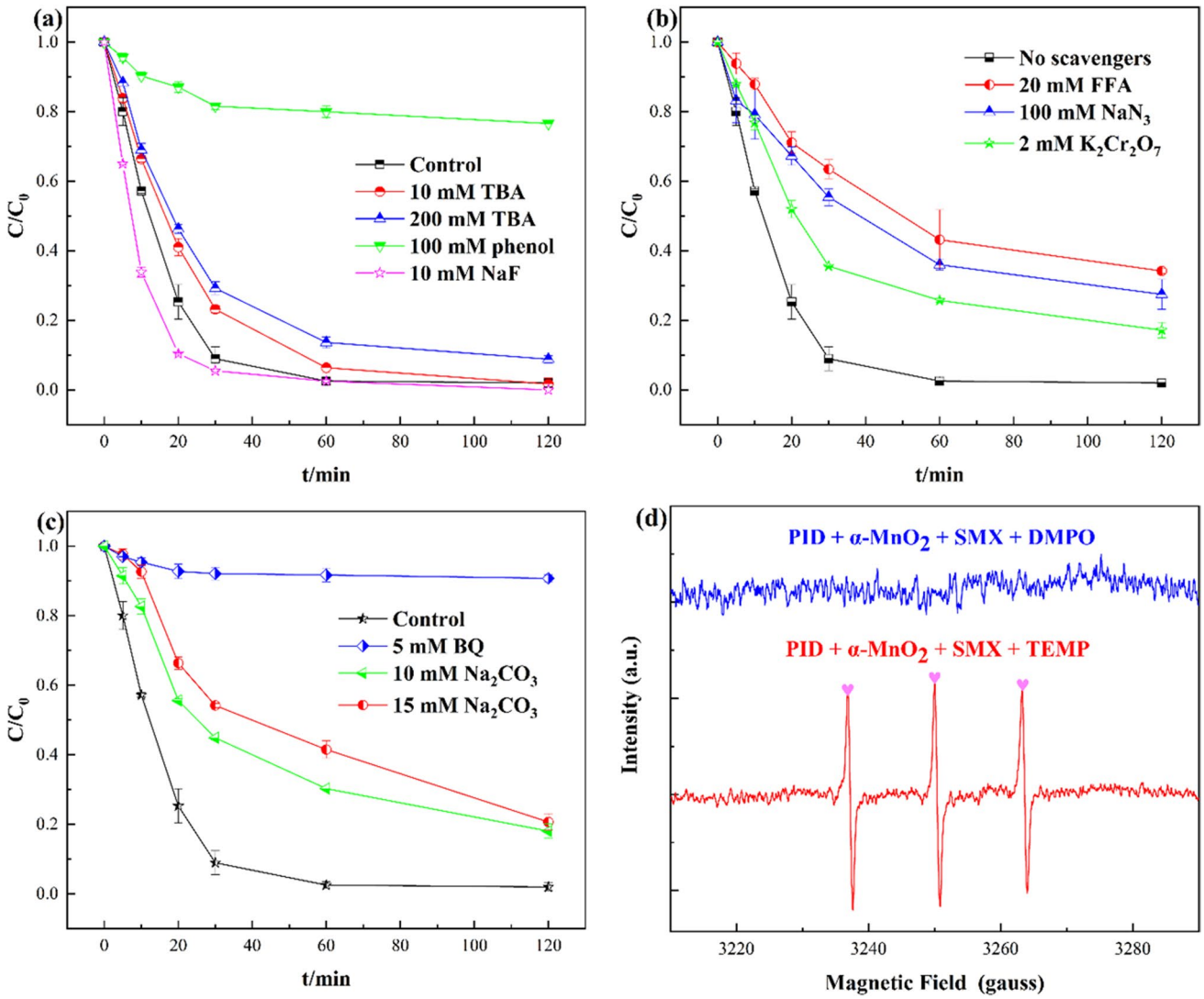

Fig. 5 Quenching effects of (a) TBA, phenol, NF, (b) FFA, $K_2Cr_2O_7$, NaN_3, (c) BQ and Na_2CO_3 in the α-MnO_2/IO_4^- process; (d) EPR spectra of TEMP and DMPO adducts in the α-MnO_2/IO_4^- system. Reaction condition: $[Sulfamethoxazole]_0 = 10$ mg/L, $[IO_4^-]_0 = 2$ mM, $[\alpha\text{-}MnO_2]_0 = 0.2$ g/L, pH = 7, [TEMP] = 0.23 g/L, [DMPO] = 100 mM

(Bokare and Choi 2015; Du et al. 2020; Sun et al. 2020). To investigate the possible role of $^1O_2$, sodium azide (($k_2(NaN_3, {}^1O_2) = 1 \times 10^9\ M^{-1}\ s^{-1}$) and furfuryl alcohol ((k_2(FFA, $^1O_2) = 1.2 \times 10^8\ M^{-1}\ s^{-1}$) were used to quench the oxidation by $^1O_2$ (Bokare and Choi 2015). The addition of azide ions and FFA caused a noticeable decline in SMX degradation rate from 0.0649 min^{-1} to 0.0106 min^{-1} and 0.0092 min^{-1}, indicating that the generation of $^1O_2$ was involved in the oxidative degradation process (Fig. 5(b)). However, sodium azide and FFA cannot only quench $^1O_2$, but also hydroxyl radicals with a second-order rate of $1.2 \times 10^{10}\ M^{-1}\ s^{-1}$ and $1.5 \times 10^{10}\ M^{-1}\ s^{-1}$, respectively. Therefore, in order to further confirm the role of $^1O_2$ in α-MnO_2/IO_4^- system, rhodamine B (RhB) was introduced to the indicator of singlet oxygen because RhB has unique degradation behaviors. When RhB was degraded by $^1O_2$, the maximum peak blue-shift would occur and continue throughout the degradation process due to the *N*-de-ethylation of RhB (Ma et al. 2020). As Fig. 6 shows, the maximum absorption peak of RhB exhibited distinct blue shift during the oxidative reaction, while other reaction systems were decreased vertically at 554 nm. Additionally, we also used the methylene blue (MB) to examine the maximum peak change because MB with conjugated *N*-ethyls has the same degradation behaviors as RhB and found that the result of MB was consistent with RhB (Fig. 6d). In addition to the above analysis, the identification of $^1O_2$ in α-MnO_2/IO_4^- process was also determined by EPR technique using DMPO as a singlet oxygen scavenger (Zhu et al. 2019). As depicted in Fig. 5d, the characteristic 1:1:1 triplet signal of TEMPOL adducts by $^1O_2$ oxidation

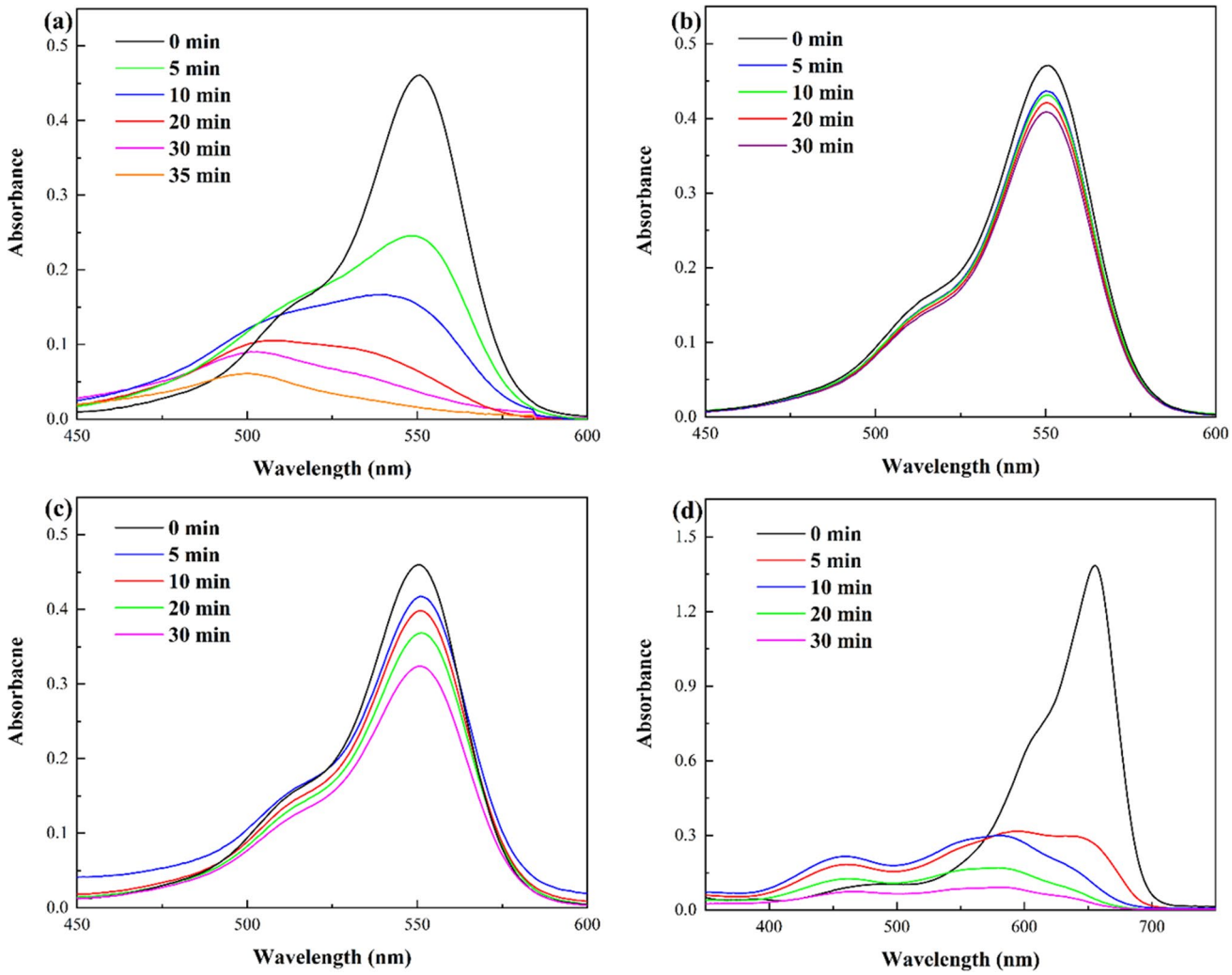

Fig. 6 Time-dependent UV-absorption spectra of degradation of RhB or MB by (a) α-MnO_2/IO_4^-/RhB, (b) α-MnO_2/RhB, (c) IO_4^-/RhB and (d) α-MnO_2/IO_4^-/MB. Reaction condition: [Rhodamine B]$_0$ = [Methylene blue]$_0$ = 10 mg/L, [IO_4^-]$_0$ = 2 mM, [α-MnO_2]$_0$ = 0.2 g/L, pH = 7

was observed, which was another specific evidence of $^1O_2$ generation. Thus, for the above results, we concluded that $^1O_2$ was generated and served as the major reactive species for SMX degradation in the α-MnO_2/IO_4^- process.

According to previous researches, the formation of $^1O_2$ can be resulted from the direct oxidation or recombination of superoxide radicals $\left(O_2^{\bullet-}\right)$, which could be generated as the reaction between IO_4^- and dissolved oxygen or produced by manganese dioxide (Chadi et al. 2019; Du et al. 2020; Zhu et al. 2019). In order to investigate the generation of $O_2^{\bullet-}$ species during the oxidation, sodium carbonate (($k_2(CO_3^{2-}, O_2^{\bullet-}) = 5 \times 10^8$ M^{-1} s^{-1}) was employed to determine the possible involvement of $O_2^{\bullet-}$ in the system (Bokare and Choi 2015). As illustrated in Fig. 5c, the SMX removal efficiency was clearly inhibited in the α-MnO_2/IO_4^- system when 10 mM and 15 mM of CO_3^{2-} were introduced, respectively. However, when the concentrations of CO_3^{2-} increased from 10 to 15 mM, the inhibitory impact of CO_3^{2-} did not show obvious change, indicating that the involvement of $O_2^{\bullet-}$ needs further confirmation. Hence, benzoquinone (($k_2\left(BQ, O_2^{\bullet-}\right) = 2.9 \times 10^9$ M^{-1} s^{-1}) was used as a more selective scavenger for $O_2^{\bullet-}$, and the SMX degradation was virtually completely inhibited by the addition of 5 mM BQ (Wang et al. 2021a, b). According to above results, we found that $O_2^{\bullet-}$ was produced in the α-MnO_2/IO_4^- system, and the quenching experiments of $O_2^{\bullet-}$ may inhibit the formation of $^1O_2$, which would lead to a reduction in the SMX degradation. Therefore, a plausible mechanism for α-MnO_2/IO_4^- activation was proposed as displayed in Eqs. 5–12 and Fig. 7. The -OH groups were first absorbed into the surface of α-MnO_2 and combined with active sites to form $\equiv MN(IV) - OH$, and then, a metastable manganese intermediate $\left(\equiv \mathrm{MN(IV)} - \mathrm{O} - \mathrm{IO}_3^-\right)$ was generated by reacting

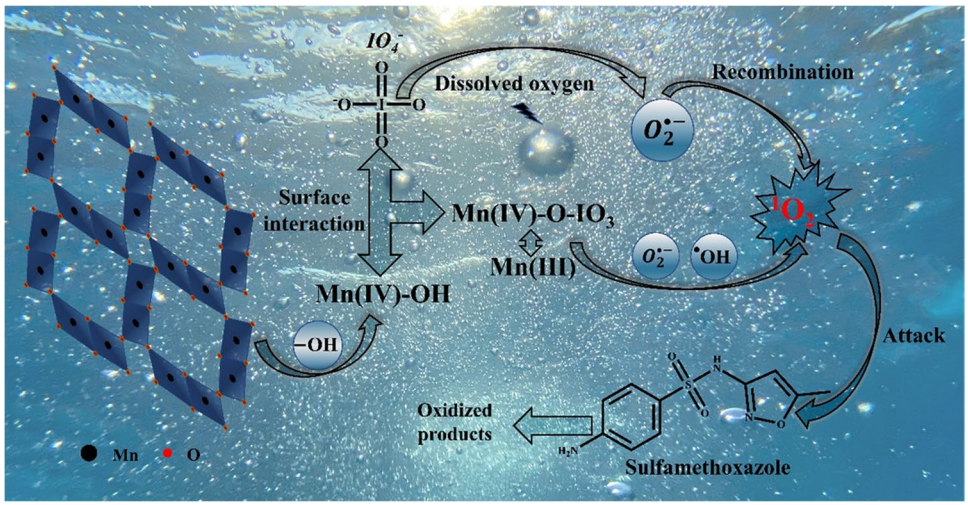

Fig. 7 The plausible mechanism of periodate activation catalyzed over α-MnO_2 for the degradation of sulfamethoxazole

with IO_4^- (Eq. 5) (Pan et al. 2021). Afterward, $O_2^{\bullet-}$ can be generated as an intermediate product through reaction of IO_4^- with dissolved oxygen (Eq. 6) (Lin and Yamada 1999). However, the SMX oxidation efficiency was not significantly suppressed with continuous N_2 purging (Fig. S12), which indicates that the formation of $O_2^{\bullet-}$ was not entirely depended on the presence of dissolved oxygen. Therefore, according to previous studies, $O_2^{\bullet-}$ can be also produced by the reaction of $\equiv MN(IV) - O - IO_3^-$ and IO_4^- along with the rupture of Mn(IV)-O (Eq. 7) (Chan et al. 2018; Du et al. 2019a, b; Zhu et al. 2019). Later, $^1O_2$ was generated from the direct oxidation of $O_2^{\bullet-}$ by Mn (IV) or residual periodate (Eqs. 7–8), which is thermodynamically favored [E_0•($^1O_2/O_2^{\bullet-}$ = -0.34 V_{NHE} and E_0 ($Mn^{(IV)}/Mn^{(III)}$) = 0.95 V_{NHE} or E_0 (IO_4^-/IO_3^-) = 0.7 V_{NHE}]. Moreover, the recombination of superoxide radicals can then generate $^1O_2$ and H_2O_2 (Eq. 10). Thus, we investigated the presence of H_2O_2 in the oxidation process by using molybdate ($(NH_4)_6Mo_7O_{24}$) because peroxomolybdic acid complex formed by H_2O_2 and molybdate has an absorption peak at 350 nm (Chai et al. 2004). Figure S13 shows that the concentration of H_2O_2 in the degradation process increased along with the magnified oxidation system, and the content of H_2O_2 exhibited a continuous enhancement in 10 min while gradually decreased after 10 min. Besides, •OH can also participate in the degradation through $O_2^{\bullet-}$ acted as a precursor to form $^1O_2$ (Eq. 11) (Chadi et al. 2019; Sun et al. 2020). In summary, this activation mechanism shows that $O_2^{\bullet-}$ and •OH were involved in $^1O_2$ generation, which played a particularly essential role in the SMX degradation.

$$\equiv Mn(IV) - OH + IO_4^- \rightarrow \equiv Mn(IV) - O - IO_3^- + OH^- \quad (5)$$

$$IO_4^- + O_2 + 2OH^- \rightarrow IO_3^- + 2O_2^- + H_2O \quad (6)$$

$$2\left[\equiv Mn(IV) - O - IO_3^-\right] + IO_4^- + 3H_2O \rightarrow 2[\equiv Mn(III) - OH] + 2O_2^- + 3IO_3^- + 4H^+ \quad (7)$$

$$\equiv Mn(IV) - O - IO_3^- + O_2^- + OH^- \rightarrow \equiv Mn(III) - OH + IO_4^- + {}^1O_2 \quad (8)$$

$$3IO_4^- + 2O_2^- + H_2O \rightarrow IO_3^- + 2{}^1O_2 + 2OH^- \quad (9)$$

$$2O_2^- + 2H_2O \rightarrow {}^1O_2 + H_2O_2 + 2OH^- \quad (10)$$

$$OH + O_2^- \rightarrow {}^1O_2 + OH^- \quad (11)$$

$${}^1O_2 + Org \rightarrow Org_{\cdot OX} \quad (12)$$

To analyze the surface properties of α-MnO_2 catalyst, the XPS spectra of pristine and treated catalysts are recorded in Fig. 8a&b. The peaks in the Mn $2p_{3/2}$ binding energies at 640.8 eV identified as Mn (III), and those at 642 eV and 643.1 eV assigned to Mn (IV) (Peng et al. 2017; Zhu et al. 2019). Compare to fresh α-MnO_2, the peak of Mn (III) was enhanced after the reaction. In addition, the deconvolution peaks of O1s show three spectral bands at 529.6 eV, 531.2 eV and 532.4 eV, representing the metal oxides, surface hydroxyl and physically adsorbed water on the surface, respectively (Tan et al. 2017; Yang et al. 2020). During the activation of periodate, the percentage of surface hydroxyl increased from 8.66% to 18.98% in the used catalyst, revealing the surface of α-MnO_2 was hydroxylated during the degradation process. In order to determine the role of surface hydroxyl groups in the oxidative reaction, phosphate ions were employed because $H_2PO_4^-$ can replace the surface hydroxyl groups through strongly bonding with the active sites (Lin et al. 2019). As shown in Fig. S14, the addition of 1 mM $H_2PO_4^-$ resulted in an obvious inhibition of SMX removal, suggesting that periodate was unable to successfully bond with active sites

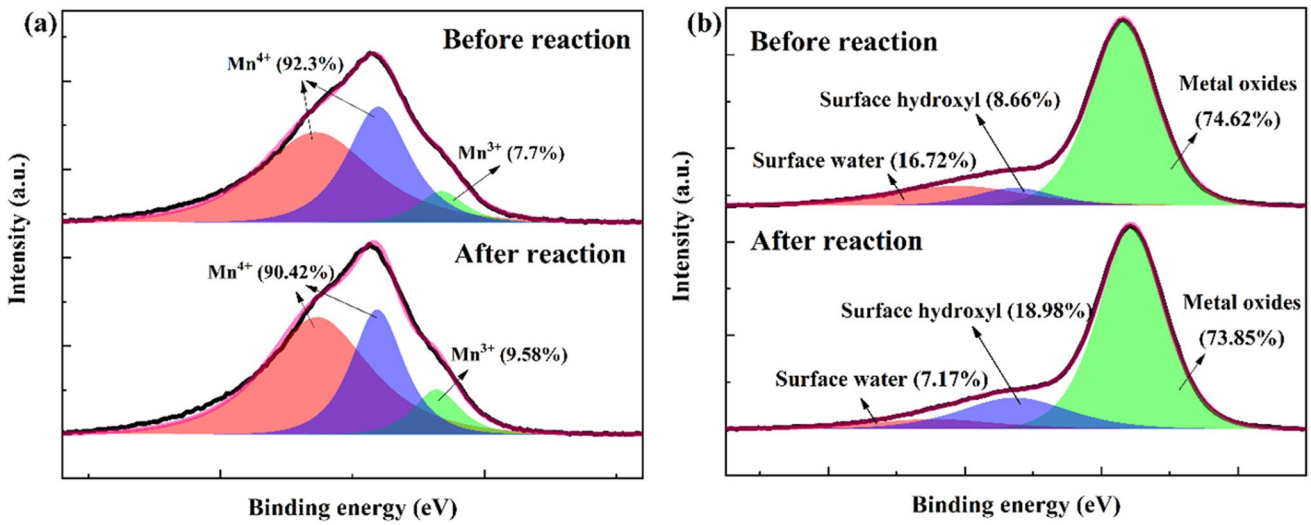

Fig. 8 XPS spectra of α-MnO_2 in the α-MnO_2/IO_4^- system before and after reaction: (a) Mn $2p_{3/2}$, and (b) O1s

via the surface hydroxyl groups when the surface hydroxyl groups were replaced by the phosphate. Meanwhile, the transformation of the surface hydroxyl groups and the alteration of surface redox states on the activator attributed to the electron transfer from IO_4^- to Mn (IV) during the generation of $^1O_2$, wherein the surface hydroxyl groups of catalyst were acted as an *outer-sphere bridge* between the periodate and α-MnO_2 (Ramaswamy and Mukerjee 2011). In addition, Fig. S16 shows the recorded cyclic voltammetry (CV) curve of α-MnO_2 during the reaction, which indicates the α-MnO_2 with a more effective redox property can make electron transfer feasible for the reaction. Moreover, the proposed mechanism with the involvement of $O_2^{\bullet-}$, $^{\bullet}OH$ and Mn (IV) intermediates was in agreement with the previous inference in Sect. 3.2. Therefore, the α-MnO_2/IO_4^- system endowed the activator with higher catalytic effect and better electron-transfer mediating ability, which could be a favorable choice for selective destruction of antibiotic pollutants (Detailed information in Text S3).

Conclusions

In summary, we performed a novel chemical oxidation process to investigate periodate activation on alpha-MnO_2, which aimed at boosting the reaction efficiency of IO_4^--based process for selective destruction of antibiotic pollutants. Among the four phases of MnO_2 catalysts, α-MnO_2 exhibited the best catalytic performance for periodate activation and SMX degradation. Under optimized conditions, about 91.05% SMX could be removed within 30 min. The degradation efficiency increased with increasing the dosages of α-MnO_2 and periodate, but the alkaline pH exerted significantly negative effect on the SMX degradation. As inferred from the quenching agents, chemical probes and EPR analysis, singlet oxygen ($^1O_2$) was unveiled be to the primary reactive oxygen species, which was generated from $O_2^{\bullet-}$ and $^{\bullet}OH$ Meanwhile, the high catalytic reactivity of α-MnO_2 can be attributed to the electron transfer through the change of manganese valence states and surface hydroxyl groups. Also, SMX and its product information were identified through three degradation pathways in α-MnO_2/IO_4^- system. This study of periodate activation by manganese dioxides will be of scientific significance in antibiotic wastewater remediation, and the understanding of advanced oxidation process by manganese-based minerals or sediment with low cost.

Supplementary Information The online version contains supplementary material available at https://doi.org/10.1007/s11356-022-18901-z.

Acknowledgements This work was supported by the National Natural Science Foundations of China (41907153, 42077312) and National Key R&D Program of China (2021YFE0106600).

Author contribution Zhijie wang contributed to performing experiments, data analyses and writing the first draft of the manuscript. Jianguo bao involved in research grant acquisition, research project administration and supervision. Jiangkun Du conducted a critical revision of the manuscript for important intellectual content, and Liting Luo analyzed the data. Guangfeng Xiao and Ting Zhou helped in the experiment and manuscript reviewing. All the authors read and approved the final manuscript.

Data availability All relevant data are within the manuscript and available from the corresponding author upon request.

Declarations

Ethics approval Not applicable.

Consent to participate Not applicable.

Consent to publication Not applicable.

Competing interests The authors declare no competing interests.

References

Antony J, Niveditha SV, Gandhimathi R, Ramesh ST, Nidheesh PV (2020) Stabilized landfill leachate treatment by zero valent aluminium-acid system combined with hydrogen peroxide and persulfate based advanced oxidation process. Waste Manag 106:1–11

Bendjama H, Merouani S, Hamdaoui O, Bouhelassa M (2018) Efficient degradation method of emerging organic pollutants in marine environment using UV/periodate process: Case of chlorazol black. Mar Pollut Bull 126:557–564

Bokare AD, Choi W (2015) Singlet-Oxygen Generation in Alkaline Periodate Solution. Environ Sci Technol 49:14392–14400

Buxton GV, Greenstock CL, Helman WP, Ross AB (1988) CRITICAL-REVIEW OF RATE CONSTANTS FOR REACTIONS OF HYDRATED ELECTRONS, HYDROGEN-ATOMS AND HYDROXYL RADICALS (.OH/.O-) IN AQUEOUS-SOLUTION. J Phys Chem Ref Data 17:513–886

Chadi NE, Merouani S, Hamdaoui O, Bouhelassa M, Ashokkumar M (2019) H2O2/periodate (IO4-): a novel advanced oxidation technology for the degradation of refractory organic pollutants. Environmental Science-Water Research & Technology 5:1113–1123

Chai XS, Hou QX, Luo Q, Zhu JY (2004) Rapid determination of hydrogen peroxide in the wood pulp bleaching streams by a dual-wavelength spectroscopic method. Anal Chim Acta 507:281–284

Chan ZM, Kitchaev DA, Weker JN, Schnedermann C, Lim K, Ceder G, Tumas W, Toney MF, Nocera DG (2018) Electrochemical trapping of metastable Mn3+ ions for activation of MnO2 oxygen evolution catalysts. Proc Natl Acad Sci USA 115:E5261–E5268

Chen H, Wang J (2021) Degradation of sulfamethoxazole by ozonation combined with ionizing radiation. J Hazard Mater 407:124377

Choi Y, Yoon HI, Lee C, Vetrakova L, Heger D, Kim K, Kim J (2018) Activation of Periodate by Freezing for the Degradation of Aqueous Organic Pollutants. Environ Sci Technol 52:5378–5385

Deng J, Ge YJ, Tan CQ, Wang HY, Li QS, Zhou SQ, Zhang KJ (2017) Degradation of ciprofloxacin using alpha-MnO2 activated peroxymonosulfate process: Effect of water constituents, degradation intermediates and toxicity evaluation. Chem Eng J 330:1390–1400

Devaraj S, Munichandraiah N (2008) Effect of crystallographic structure of MnO2 on its electrochemical capacitance properties. J Phys Chem C 112:4406–4417

Du J, Bao J, Liu Y, Kim SH, Dionysiou DD (2019a) Facile preparation of porous Mn/Fe3O4 cubes as peroxymonosulfate activating catalyst for effective bisphenol A degradation. Chemical Engineering Journal, 376.

Du J, Tang S, Faheem LH, Zheng H, Xiao G, Luo L, Bao J (2019) Insights into periodate oxidation of bisphenol A mediated by manganese. Chem Eng J 369:1034–1039

Du J, Xiao G, Xi Y, Zhu X, Su F, Kim SH (2020) Periodate activation with manganese oxides for sulfanilamide degradation. Water Res 169:115278

Gozmen B, Turabik M, Hesenov A (2009) Photocatalytic degradation of Basic Red 46 and Basic Yellow 28 in single and binary mixture by UV/TiO2/periodate system. J Hazard Mater 164:1487–1495

Guo R, Nengzi LC, Chen Y, Li Y, Zhang X, Cheng X (2020) Efficient degradation of sulfamethoxazole by CuCo LDH and LDH@fibers composite membrane activating peroxymonosulfate. Chemical Engineering Journal, 398.

Huang J, Zhong S, Dai Y, Liu CC, Zhang H (2018) Effect of MnO2 Phase Structure on the Oxidative Reactivity toward Bisphenol A Degradation. Environ Sci Technol 52:11309–11318

Huang KZ, Zhang HC (2019) Direct Electron-Transfer-Based Peroxymonosulfate Activation by Iron-Doped Manganese Oxide (delta-MnO2) and the Development of Galvanic Oxidation Processes (GOPs). Environ Sci Technol 53:12610–12620

Huang Y, Nengzi LC, Li X, Meng L, Song Q, Cheng X (2020) Fabrication of Cu2O/Bi25FeO40 nanocomposite and its enhanced photocatalytic mechanism and degradation pathways of sulfamethoxazole. Materials Science in Semiconductor Processing, 109.

Jia JB, Zhang PY, Chen L (2016) Catalytic decomposition of gaseous ozone over manganese dioxides with different crystal structures. Applied Catalysis B-Environmental 189:210–218

Lalas K, Petala A, Frontistis Z, Konstantinou I, Mantzavinos D (2021) Sulfamethoxazole degradation by the CuOx/persulfate system. Catal Today 361:139–145

Lee H, Yoo HY, Choi J, Nam IH, Lee S, Lee S, Kim JH, Lee C, Lee J (2014) Oxidizing capacity of periodate activated with iron-based bimetallic nanoparticles. Environ Sci Technol 48:8086–8093

Lee YC, Chen MJ, Huang CP, Kuo J, Lo SL (2016) Efficient sonochemical degradation of perfluorooctanoic acid using periodate. Ultrason Sonochem 31:499–505

Li Q, Huang X, Su G, Zheng M, Huang C, Wang M, Ma C, Wei D (2018) The Regular/Persistent Free Radicals and Associated Reaction Mechanism for the Degradation of 1,2,4-Trichlorobenzene over Different MnO2 Polymorphs. Environ Sci Technol 52:13351–13360

Li XW, Liu XT, Lin CY, Qi CD, Zhang HJ, Ma J (2017) Enhanced activation of periodate by iodine-doped granular activated carbon for organic contaminant degradation. Chemosphere 181:609–618

Li Y, He J, Zhang K, Hong P, Wang C, Kong L, Liu J (2020) Oxidative degradation of sulfamethoxazole antibiotic catalyzed by porous magnetic manganese ferrite nanoparticles: mechanism and by-products identification. J Mater Sci 55:13767–13784

Li Y, Li J, Pan Y, Xiong Z, Yao G, Xie R, Lai B (2020b) Peroxymonosulfate activation on FeCo2S4 modified g-C3N4 (FeCo2S4-CN): Mechanism of singlet oxygen evolution for nonradical efficient degradation of sulfamethoxazole. Chemical Engineering Journal, 384.

Lin H, Li SM, Deng B, Tan WH, Li RM, Xu Y, Zhang H (2019) Degradation of bisphenol A by activating peroxymonosulfate with Mn0.6Zn0.4Fe2O4 fabricated from spent Zn-Mn alkaline batteries. Chem Eng J 364:541–551

Lin JM, Yamada M (1999) Oxidation reaction between periodate and polyhydroxyl compounds and its application to chemiluminescence. Anal Chem 71:1760–1766

Liu CS, Zhang LJ, Feng CH, Wu CA, Li FB, Li XZ (2009) Relationship between oxidative degradation of 2-mercaptobenzothiazole and physicochemical properties of manganese (hydro)oxides. Environ Chem 6:83–92

Long Y, Dai J, Zhao S, Su Y, Wang Z, Zhang Z (2021) Atomically Dispersed Cobalt Sites on Graphene as Efficient Periodate Activators for Selective Organic Pollutant Degradation. Environ Sci Technol.

Ma JH, Guo RR, Tan XN (2020) Aqueous photochemistry of fullerol revisited: Energy transfer vs. electron transfer processes probed by Rhodamine B degradation. Journal of Photochemistry and Photobiology a-Chemistry, 397.

Oh W-D, Dong Z, Lim T-T (2016) Generation of sulfate radical through heterogeneous catalysis for organic contaminants removal: Current development, challenges and prospects. Appl Catal B 194:169–201

Pan F, Ji H, Du P, Huang T, Wang C, Liu W (2021) Insights into catalytic activation of peroxymonosulfate for carbamazepine degradation by MnO2 nanoparticles in-situ anchored titanate nanotubes: Mechanism ecotoxicity and DFT study. J Hazard Mater 402:123779

Peng X, Guo YQ, Yin Q, Wu JC, Zhao JY, Wang CM, Tao S, Chu WS, Wu CZ, Xie Y (2017) Double-Exchange Effect in Two-Dimensional MnO2 Nanomaterials. J Am Chem Soc 139:5242–5248

Qi CD, Liu XT, Lin CY, Zhang XH, Ma J, Tan HB, Ye W (2014) Degradation of sulfamethoxazole by microwave-activated persulfate: Kinetics, mechanism and acute toxicity. Chem Eng J 249:6–14

Ramaswamy N, Mukerjee S (2011) Influence of Inner- and Outer-Sphere Electron Transfer Mechanisms during Electrocatalysis of Oxygen Reduction in Alkaline Media. J Phys Chem C 115:18015–18026

Saputra E, Muhammad S, Sun H, Ang HM, Tade MO, Wang S (2013) Different crystallographic one-dimensional MnO2 nanomaterials and their superior performance in catalytic phenol degradation. Environ Sci Technol 47:5882–5887

Saputra E, Muhammad S, Sun HQ, Patel A, Shukla P, Zhu ZH, Wang SB (2012) alpha-MnO2 activation of peroxymonosulfate for catalytic phenol degradation in aqueous solutions. Catal Commun 26:144–148

Seid-Mohammadi A, Asgari G, Shokoohi R, Baziar M, Mirzaei N, Adabi S, Partoei K (2019) Degradation of phenol using US/periodate/nZVI system from aqueous solutions. Global NEST J 21:360–367

Sun HW, He F, Choi WY (2020) Production of Reactive Oxygen Species by the Reaction of Periodate and Hydroxylamine for Rapid Removal of Organic Pollutants and Waterborne Bacteria. Environ Sci Technol 54:6427–6437

Tan XQ, Wan YF, Huang YJ, He C, Zhang ZL, He ZY, Hu LL, Zeng JW, Shu D (2017) Three-dimensional MnO2 porous hollow microspheres for enhanced activity as ozonation catalysts in degradation of bisphenol A. J Hazard Mater 321:162–172

Taujale S, Baratta LR, Huang J, Zhang H (2016) Interactions in Ternary Mixtures of MnO2, Al2O3, and Natural Organic Matter (NOM) and the Impact on MnO2 Oxidative Reactivity. Environ Sci Technol 50:2345–2353

Wang JL, Wang SZ (2020) Reactive species in advanced oxidation processes: Formation, identification and reaction mechanism. Chemical Engineering Journal, 401.

Wang Q, Zeng H, Liang YH, Cao Y, Xiao Y, Ma J (2021) Degradation of bisphenol AF in water by periodate activation with FeS (mackinawite) and the role of sulfur species in the generation of sulfate radicals. Chem Eng J 407:11

Wang Q, Zeng H, Liang YH, Cao Y, Xiao Y, Ma J (2021b) Degradation of bisphenol AF in water by periodate activation with FeS (mackinawite) and the role of sulfur species in the generation of sulfate radicals. Chemical Engineering Journal, 407.

Wang SZ, Liu Y, Wang JL (2020) Peroxymonosulfate Activation by Fe-Co-O-Codoped Graphite Carbon Nitride for Degradation of Sulfamethoxazole. Environ Sci Technol 54:10361–10369

Wang YX, Indrawirawan S, Duan XG, Sun HQ, Ang HM, Tade MO, Wang SB (2015) New insights into heterogeneous generation and evolution processes of sulfate radicals for phenol degradation over one-dimensional alpha-MnO2 nanostructures. Chem Eng J 266:12–20

Xu YM, Lv KL, Xiong ZG, Leng WH, Du WP, Liu D, Xue XJ (2007) Rate enhancement and rate inhibition of phenol degradation over irradiated anatase and rutile TiO2 on the addition of NaF: New insight into the mechanism. J Phys Chem C 111:19024–19032

Yang SY, Xiao T, Zhang J, Chen YY, Li L (2015) Activated carbon fiber as heterogeneous catalyst of peroxymonosulfate activation for efficient degradation of Acid Orange 7 in aqueous solution. Sep Purif Technol 143:19–26

Yang WH, Su ZA, Xu ZH, Yang WN, Peng Y, Li JH (2020) Comparative study of alpha-, beta-, gamma- and delta-MnO2 on toluene oxidation: Oxygen vacancies and reaction intermediates. Applied Catalysis B-Environmental, 260.

Yazdanbakhsh A, Eslami A, Massoudinejad M, Avazpour M (2020) Enhanced degradation of sulfamethoxazole antibiotic from aqueous solution using Mn-WO3/LED photocatalytic process: Kinetic, mechanism, degradation pathway and toxicity reduction. Chemical Engineering Journal, 380.

Zhu SS, Li XJ, Kang J, Duan XG, Wang SB (2019) Persulfate Activation on Crystallographic Manganese Oxides: Mechanism of Singlet Oxygen Evolution for Nonradical Selective Degradation of Aqueous Contaminants. Environ Sci Technol 53:307–315

Zong Y, Shao Y, Zeng Y, Shao B, Xu L, Zhao Z, Liu W, Wu D (2021) Enhanced Oxidation of Organic Contaminants by Iron(II)-Activated Periodate: The Significance of High-Valent Iron-Oxo Species. Environ Sci Technol.